CHEMISTRY
A EUROPEAN JOURNAL

DOI: 10.1002/chem.200801827

Complexation between Methyl Viologen (Paraquat) Bis(Hexafluorophosphate) and Dibenzo[24]Crown-8 Revisited

Travis B. Gasa,[a] Jason M. Spruell,[a] William R. Dichtel,[b] Thomas J. Sørensen,[c] Douglas Philp,[d] J. Fraser Stoddart,*[a] and Petr Kuzmič*[e]

Abstract: Paraquat bis(hexafluorophosphate) undergoes stepwise dissociation in acetone. All three species—the neutral molecule, and the mono- and dications—are represented significantly under the experimental conditions typically used in host–guest binding studies. Paraquat forms at least four host–guest complexes with dibenzo[24]crown-8. They are characterized by both 1:1 and 1:2 stoichiometries, and an overall charge of either zero (neutral molecule) or one (monocation). The monocationic 1:1 host–guest complex is the most abundant species under typical (0.5–20 mM) experimental conditions. The presence of the dicationic 1:1 host–guest complex cannot be excluded on the basis of our experimental data, but neither is it unambiguously confirmed to be present. The two confirmed forms of paraquat that do undergo complexation—the neutral molecule and the monocation—exhibit approximately identical binding affinities toward dibenzo[24]crown-8. Thus, the relative abundance of neutral, singly, and doubly charged pseudorotaxanes is identical to the relative abundance of neutral, singly, and doubly charged paraquat unbound with respect to the crown ether in acetone. In the specific case of paraquat/dibenzo[24]crown-8, ion-pairing does not contribute to host–guest complex formation, as has been suggested previously in the literature.

Keywords: crown compounds · donor–acceptor systems · ion pairs · paraquat · supramolecular chemistry

Introduction

The rational design of functional mechanically interlocked molecules[1] is predicated on a precise understanding of the strengths of the noncovalent bonding interactions that exist between the matching components. Accurately quantifying the strengths of these interactions allows the design of highly programmed molecular structures with desired properties—for example, bistability, electronic, mechanical, and so forth—from simple experiments carried out on these matching components in solution prior to incorporation into the final molecular structures. For example, the equilibrium populations of the co-conformers[2] of bistable [2]rotaxanes remain consistent across solution, self-assembled monolayers (SAMs), and device environments,[3] and can be predicted from simple isothermal titration calorimetry measurements on the corresponding pseudorotaxane components in the solution phase.

The ability to correlate device performance using the power of template-directed synthesis and the precision associated with physical organic chemistry is presently one of the fundamental goals in molecular electronics. In the course of our research efforts to identify suitable recognition

[a] T. B. Gasa, J. M. Spruell, J. F. Stoddart
Department of Chemistry
Northwestern University
2145 Sheridan Road, Evanston, IL 60208 (USA)
Fax: (+1) 847-491-1009
E-mail: stoddart@northwestern.edu

[b] W. R. Dichtel
Department of Chemistry and Chemical Biology
Cornell University, 328 Baker Laboratory
Ithaca, NY 14953 (USA)

[c] T. J. Sørensen
Nano-Science Center, University of Copenhagen
Universitetsparken 5, 2100 Copenhagen Ø (Denmark)

[d] D. Philp
Centre for Biomolecular Sciences
School of Chemistry, University of St Andrews
North Haugh, St Andrews KY16 9ST (United Kingdom)

[e] P. Kuzmič
BioKin Ltd, 15 Main Street, Suite 232
Watertown, MA 02472 (USA)
Fax: (+1) 617-209-1616
E-mail: pksci01@biokin.com

Supporting information for this article is available on the WWW under http://dx.doi.org/10.1002/chem.200801827.

units for matching rings along the rod sections of the dumbbell components in new bistable rotaxanes for incorporation into molecular electronic and molecular logic devices,[1d,4] we conducted various binding studies between a neutral host, dibenzo[24]crown-8 (DB24C8), and a dicationic guest, *N*,*N*′-dimethyl-4,4′-bipyridinium (paraquat) bis(hexafluorophosphate), in acetone using both ^{1}H nuclear magnetic resonance (NMR) and ultraviolet/visible (UV/Vis) spectroscopy.

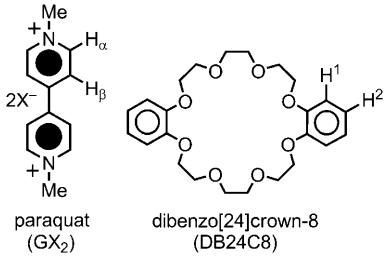

In general, ion-pairing effects can be important factors in host–guest association processes.[5] However, a detailed quantitative treatment of these effects for specific host–guest systems is rarely undertaken, because of the proliferation of simultaneous equilibria that have to be taken into account.

For example, solutions of paraquat bis(hexafluorophosphate) in [D_6]acetone have been previously modeled to contain only two states, that is, the dication and the neutral molecule.[6] It was assumed that the paraquat monocation—which is bound to only one PF_6^- counterion—is not present in [D_6]acetone.[6] The association between DB24C8 and paraquat in [D_6]acetone was also reported to be strictly of a 1:1 stoichiometry.[6] Unbound paraquat in [D_6]acetone was presumed to be fully ion-paired, whereas the DB24C8/paraquat 1:1 complex was assigned to be fully dissociated, that is, it is a dication. No singly charged host–guest complexes were included in the treatment.

In this paper, we present UV/Vis and NMR experimental evidence that contradicts these conclusions in many respects. Firstly, we show that all three possible forms of paraquat exist in acetone solution. In fact, the previously overlooked paraquat monocation is the most abundant species present at total concentrations typically used for host–guest binding studies. Secondly, we have obtained experimental evidence for the existence of a DB24C8/paraquat complex with 2:1 stoichiometry. Thirdly, our quantitative analysis of the numerous equilibria associated with the simultaneous formation of different complexes shows that the different species of paraquat have approximately identical affinities for DB24C8. This observation implies that the same extent of ion-pairing is being observed for paraquat, both when it is unbound in solution, and when it is bound to the crown ether. The most abundant host–guest complex is the DB24C8/paraquat monocation (1:1), just as the most abundant species present in solutions of unbound paraquat in acetone is singly charged. Thus, in the particular case of DB24C8/paraquat binding interactions, ion-pairing does not strongly influence or "drive" the formation of host–guest complexes as was proposed previously.[6]

Computational Methods

Complex simultaneous equilibria: The mathematical formalism used in our analysis to describe a complex mixture at equilibrium is a modification of the algorithm EQUIL.[8] It applies to an arbitrary binding (complexation) model, regardless of the number of participating molecular species, the number of steps in the reaction model, or the stoichiometries of the molecular complexes. Full mathematical details of this mathematical formalism are included in the Supporting Information.

Briefly, the theoretical model for the chemical shift of each particular aromatic proton is represented by Equation (1), in which $\delta_{obs}^{(X)}$ is the experimentally observed chemical shift of proton X in the given solution mixture, n_X is the number of distinct molecular species (both free in solution and bound in complexes) in which the particular proton appears, $\delta_i^{(X)}$ is the intrinsic chemical shift of proton X in the ith molecular species, and $c_i^{(X)}$ is the concentration of this molecular species at equilibrium. Equation (1) expresses the fact that the NMR chemical shift is an intensive physical variable. The intrinsic chemical shifts $\delta_i^{(X)}$ were treated as adjustable model parameters. All equilibrium constants appearing in each molecular mechanism were also treated as adjustable parameters. In Equation (1), these equilibrium constants are implicitly contained in the equilibrium concentrations $c_i^{(X)}$. The equilibrium concentrations $c_i^{(X)}$ were computed by a general numerical method described in the Supporting Information.

$$\delta_{obs}^{(x)} = \sum_{i=1}^{n_X} \delta_i^{(X)} c_i^{(X)} / \sum_{i=1}^{n_X} c_i^{(X)} \qquad (1)$$

Statistical analysis and model discrimination: The software program DynaFit[9] was used in all quantitative analyses. Experimentally observed chemical shifts were subjected to nonlinear least-squares regression using Equation (1) as the fitting model. Signals for all protons were combined and analyzed simultaneously in a global fit.[10] The fitting algorithm was either Reich's modification[11] of the Levenberg–Marquardt algorithm,[12] or the globally convergent differential evolution algorithm as described by Price et al.[13] Nonsymmetrical confidence intervals for optimized model parameters—equilibrium constants and chemical shifts—were estimated at the 95% confidence level by using the profile-t method of Bates and Watts.[14] Model discrimination analysis was based on the second-order Akaike information criterion (AIC_c).[15]

Results

UV/Vis spectra of DB24C8/paraquat charge-transfer complexes: UV/Vis spectra of DB24C8/paraquat mixtures in acetone contain a characteristic charge-transfer (CT) band associated with the electronic interaction between the aromatic rings on the host (H) and guest (G) molecules. When paraquat bis(hexafluorophosphate) ($[GX_2]_o$) is held at 1.02 mM, increasing amounts of DB24C8 ($[H]_o$) initially result (Figure 1, top) in the appearance of a CT band at 393 nm. As the $[H]_o$ concentration is increased further such that $[GX_2]_o$ is in excess, the absorption λ_{max} hypsochromically shifts to 378 nm. This effect is best observed when the absorbances at various wavelengths are plotted (Figure S1 in the Supporting Information) as a function of $[H]_o$. The absorbances at 350, 365, and 375 nm increase disproportionate-

ly relative to those at 393 or 405 nm. In contrast, when $[H]_o$ is held constant (1.01 mM) and $[GX_2]_o$ is increased to being in excess, only the 393 nm CT complex is observed (Figure 1, bottom). Because this second blue-shifted absorbance is only observed when $[H]_o$ is in large excess with respect to $[GX_2]_o$, we attribute this phenomenon to the formation of DB24C8/paraquat complexes with 2:1 stoichiometries.

A Job plot[16] constructed from the UV/Vis data, through observation of the intensities of the CT bands at 378 and 393 nm, showed skewing along the DB24C8 mole fraction axis towards 0.67, suggesting the formation of 2:1 (DB24C8/paraquat) complexes in solution. The 3D absorbance surface (Figure 2) suggests a stoichiometry greater than 1:1. There is also a hypsochromic shift of the absorbance which we ascribe to the formation of a 2:1 complex.

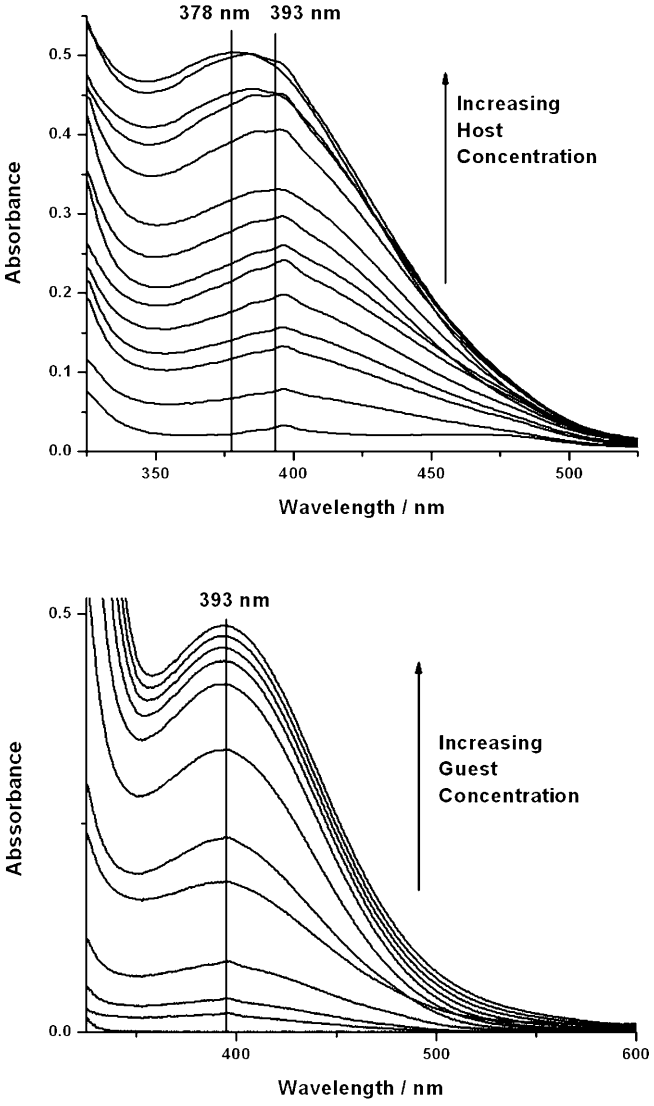

Figure 1. UV/Vis spectra of DB24C8/paraquat mixtures. Top: Hypsochromic shift of charge-transfer absorbance when $[DB24C8]_o$ is in excess in comparison with $[GX_2]_o$. Bottom: Only 393 nm charge-transfer absorbance is observed when $[GX_2]_o$ is in excess compared with $[DB24C8]_o$.

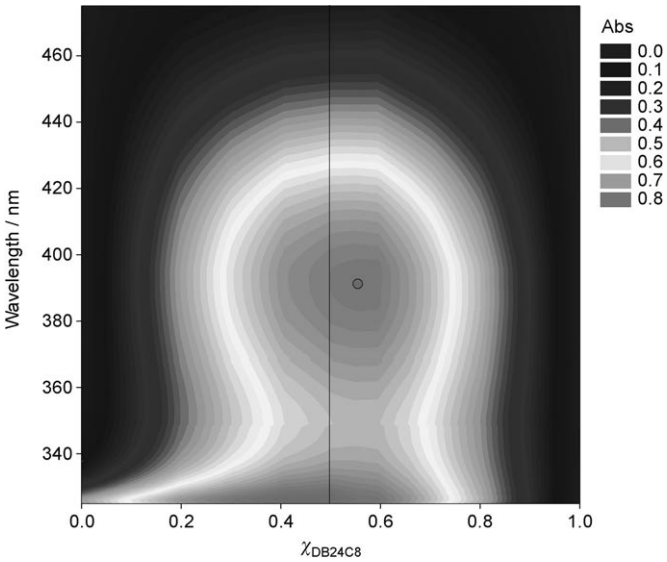

Figure 2. Three-dimensional UV/Vis Job plot of DB24C8/paraquat mixtures revealing both a skewing of the maximum absorbance towards 0.67 mole fraction of DB24C8, as well as a hypsochromic shift of the absorbance λ_{max}; both features indicative of the presence of 2:1 DB24C8/paraquat complexes.

Determination of paraquat ionization constants: When paraquat bis(hexafluorophosphate) is diluted progressively in $[D_6]$acetone, the resonances of both aromatic protons shift (Figure 3 A,B) downfield by approximately 0.1 ppm in the ^{1}H NMR spectrum. The reverse is true (Figure 3 C,D) when additional hexafluorophosphate counterions—as the tetrabutylammonium salt, Bu_4NPF_6—are added to a solution of paraquat in $[D_6]$acetone. We interpret these changes in chemical shifts to be a consequence of altering the relative abundances of the three different states of paraquat, namely, the neutral species, and the mono- and dications. We have utilized this behavior to determine the equilibrium constants for the ion-pairing processes in solution.[17]

The paraquat dilution and counterion titration data in Figure 3 were fitted to a mathematical model corresponding to the ionization model shown in Scheme 1, in which G^{2+}

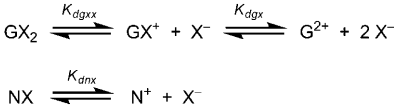

Scheme 1. Simultaneous binding processes occurring in a solution of paraquat bis(hexafluorophosphate) (GX_2) and tetrabutylammonium hexafluorophosphate (NX).

represents the paraquat dication, N^+ is the tetrabutylammonium cation, and X^- is the hexafluorophosphate anion. The equilibrium constants K_{dgxx}, K_{dgx}, and K_{dnx} are binary (stepwise) dissociation constants of the appropriate complex. This system consists of three component molecular species (G^{2+}, N^+, and X^-) and the three molecular complexes they form (GX_2, GX^+, and NX). The system of simultaneous

nonlinear algebraic equations that describe the composition at equilibrium under any given set of total concentrations of components was automatically derived by the software DynaFit;[9] the details of the mathematical formalism are described in the Supporting Information.

The best-fit values of the equilibrium constants for stepwise dissociation, as determined by the least-squares fit of chemical shift data in Figure 3, are $K_{dgxx} = (10.6 \pm 1.9)$ mM and $K_{dgx} = (0.6 \pm 0.2)$ mM; the best-fit value of the dissociation constant for Bu_4NX was $K_{dnx} = (11.1 \pm 2.7)$ mM—see Table 1, which also lists the 95% confidence intervals. We used the best-fit numerical values of the paraquat dissociation constants to simulate the relative abundance of all three species at equilibrium, at various total concentrations. The results show (Figure 4) that all three states—neutral molecule and the mono- and dications—are significantly populated in host–guest binding experiments under typical experimental conditions, with total paraquat concentrations approximately in the 1–30 mM range. In fact, the monocation (GX^+) is the most abundant species at total concentrations between 0.5–20 mM. The DynaFit[9] script that was used for this numerical simulation is listed in the Supporting Information.

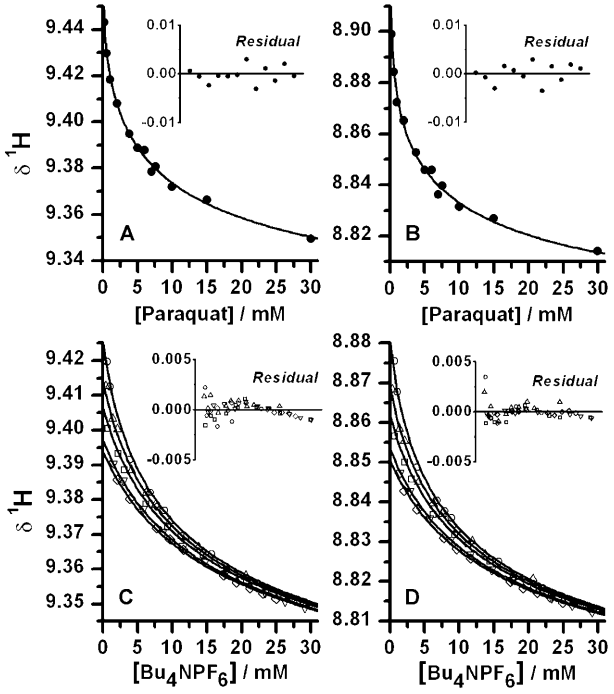

Figure 3. Least-squares fit of paraquat chemical shifts to reaction mechanism shown in Scheme 1. Left-hand panels (A, C): downfield aromatic proton H_α; right-hand panels (B, D): upfield aromatic proton H_β. Upper row (panels A, B): concentration of paraquat was varied in the absence of additional Bu_4NPF_6. Bottom row (panels C, D): concentration of additional Bu_4NPF_6 was varied, while the concentration of paraquat was held constant at 0.714 mM (○), 1.429 mM (△), 2.143 mM (□), 3.036 mM (▽), and 4.0 mM (◇). The smooth curves represent the best-fit model generated from mechanism B, defined by a system of simultaneous nonlinear algebraic equations [Supporting Information Eqs (2)–(4)]. Data shown in all four panels were analyzed simultaneously (global fit[10]).

Table 1. Best fit values, formal standard errors, and confidence intervals ("low", "high", at the 95% confidence level) of adjustable model parameters determined by DynaFit[9] from experimental data shown in Figure 3.

Parameter	Fitted	Std. Error	$Low_{95\%}$	$High_{95\%}$
K_{dgxx}[a] [mM]	10.6	1.9	7.7	17.4
K_{dgx}[a] [mM]	0.60	0.21	0.25	1.16
K_{dnx}[a] [mM]	11.1	2.7	7.2	21.7
δ[b] $H_\alpha^{(G^{2+})}$ [ppm]	9.461	0.003	–	–
δ[b] $H_\alpha^{(GX^+)}$ [ppm]	9.415	0.006	–	–
δ[b] $H_\alpha^{(GXX)}$ [ppm]	9.298	0.003	–	–
δ[b] $H_\beta^{(G^{2+})}$ [ppm]	8.919	0.004	–	–
δ[b] $H_\beta^{(GX^+)}$ [ppm]	8.866	0.006	–	–
δ[b] $H_\beta^{(GXX)}$ [ppm]	8.770	0.002	–	–

[a] Stepwise (binary) dissociation constants appearing in Scheme 1. [b] Intrinsic chemical shifts of paraquat aromatic protons in all three possible species (neutral molecule GX_2, monocation GX^+, dication G^{2+}).

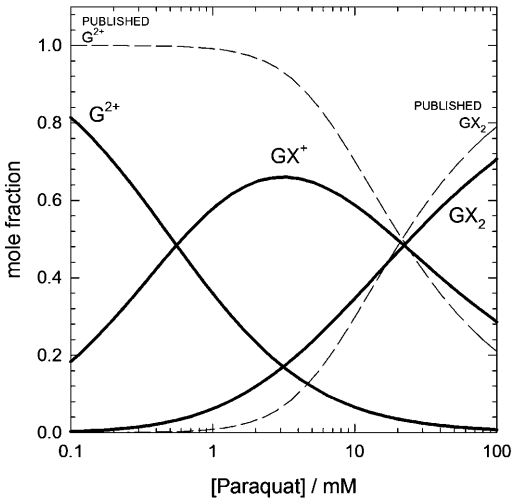

Figure 4. Mole-fraction distribution of paraquat species in acetone. The solid mole-fraction curves were simulated by using the software DynaFit,[9] while assuming that the dissociation constants K_{dgxx} and K_{dgx} (Scheme 1) have the numerical values listed in Table 1. The dashed mole-fraction curves were simulated while assuming that the dissociation of paraquat proceeds in a single step and is characterized by the total stability constant reported by Huang et al.[6]

The experimental data shown in Figure 3 were also fitted to the single-step ionization mechanism, $GX_2 \rightleftharpoons G^{2+} + 2X^-$, originally proposed by Huang et al.[6] As measured both by the AIC_c[18] and by the visual examination of the residuals of fit, the single-step ionization model failed to describe our data adequately. The results of an attempted fit to the Huang et al.[6] single-step ionization model are shown in Figure 5. The residuals are distinctly non-random, especially at relatively high concentrations of added counterion (Figure 5C,D, inset). We are obliged to conclude that the previously proposed[6] single-step dissociation mechanism for paraquat dissociation in acetone is in conflict with our experimental data.

NMR spectroscopy of DB24C8/paraquat complexes: Paraquat, DB24C8, and Bu_4NPF_6 were mixed in [D_6]acetone at various total concentrations, and the chemical shifts of all

four aromatic protons were determined for each ternary mixture. Four series of experiments were performed, each at a different total concentration of the counterion, $[Bu_4NPF_6]_o = 1$, 6, 12, and 24 mM. Within each series, the total concentrations of paraquat and DB24C8 were varied such that the sum of concentrations remained the same, $[GX_2 + DB24C8]_o = 12$, 9, 6, and 3 mM. The mole fractions in each series were $X_{DB24C8} = 0.1$, 0.25, 0.5, 0.75, and 0.9. Each sample was prepared in duplicate, giving a total of 40 independent chemical shift measurements for each of the four protons. The complete data set contained 153 data points. The standard deviations of chemical shifts from the replicated measurements ranged between 0.001 and 0.006 ppm and the median standard deviation from all replicates was 0.002 ppm. The numerical values of all chemical shifts are listed in the Supporting Information and displayed graphically in Figure 6.

Considering the binding steps displayed in Scheme 2, there exist exactly 26 possible pathways or mechanisms for DB24C8 and paraquat—in any of its three states—to form either 1:1 or 2:1 complexes. We have used the DynaFit software[9] to construct all 26 mathematical models corresponding to each binding mechanism, and performed the least-squares fit (Figure 6) of the chemical shift data to all of the theoretical models in turn. We also considered the DB24C8/paraquat complexation mechanism previously proposed by Huang et al.[6] Finally, we included three degenerate fitting models, in which the numerical values of certain pairs of equilibrium constants were forced to be identical. The complete list of all 30 binding mechanisms that we examined is given in Table 2 and in the Supporting Information. Model 1 in Table 2 is the previously proposed model,[6] while models 27–30 are the three degenerate models.

In the first-pass model discrimination analysis, we examined three independent characteristics of each candidate fitting model in order to decide whether or not to accept a given model for further consideration.

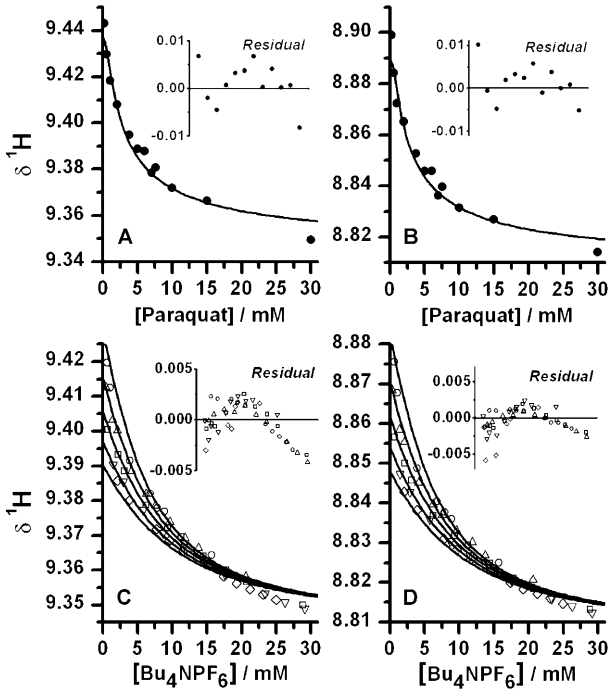

Figure 5. Least-squares fit of paraquat chemical shifts to the single-step dissociation mechanism ($GX_2 \rightleftharpoons G^{2+} + 2X^-$) proposed by Huang et al.[6] See legend to Figure 3 for other details.

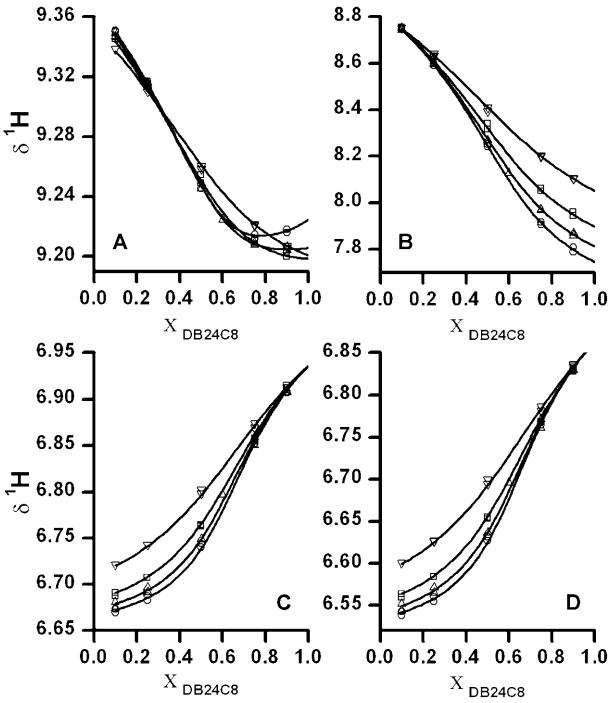

Figure 6. Least-squares fit of paraquat and DB24C8 chemical shifts. A) upfield proton (H_β) on paraquat; B) downfield proton (H_α) on paraquat; C) upfield proton (H^2) on DB24C8; D) downfield proton (H^1) on DB24C8. Horizontal axis: mole fraction of DB24C8. ○: $[Bu_4NPF_6]_o = 1$ mM, $[GX_2 + DB24C8]_o = 12$ mM; △: $[Bu_4NPF_6]_o = 6$ mM, $[GX_2 + DB24C8]_o = 9$ mM; □: $[Bu_4NPF_6]_o = 12$ mM, $[GX_2 + DB24C8]_o = 6$ mM; ▽: $[Bu_4NPF_6]_o = 24$ mM, $[GX_2 + DB24C8]_o = 3$ mM. In each series of data points, the mole fraction of DB24C8 was 0.1, 0.25, 0.5, 0.75, and 0.9. Data shown in all four panels (153 chemical shifts) were analyzed simultaneously (global fit[10]). The smooth curves represent the best-fit model curves generated from the reaction mechanism model 29 in Table 2 (see also Scheme 2). The 95% confidence intervals of equilibrium constants appearing in model 29 are listed in Table 3.

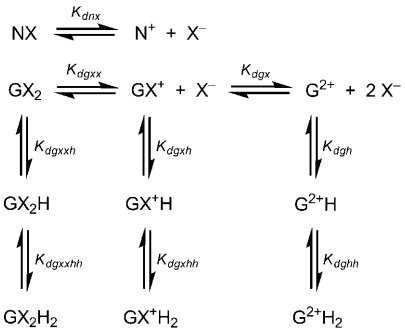

Scheme 2. All possible simultaneous binding processes occurring in a solution of paraquat bis(hexafluorophosphate) (GX_2), tetrabutylammonium hexafluorophosphate (NX), and dibenzo[24]crown-8 (H).

Table 2. First-pass model discrimination analysis for 30 possible DB24C8/paraquat binding mechanisms.

Model	K_{dgxx}[a]	K_{dgx}[a]	K_{dgxxh}[a]	K_{dgxxhh}[a]	K_{dgxh}[a]	K_{dgxhh}[a]	K_{dgh}[a]	K_{dghh}[a]	Weight[b]	Errors[c]	Shifts[d]	$Pass_{1\%}$[e]	$Pass_{5\%}$[e]	$Pass_{10\%}$[e]
1	+	n/a					+		0	+	+			
2	+	+					+		0	+	+			
3	+	+					+	+	0	+	+			
4	+	+			+				0	+	+			
5	+	+			+	+			0	+	+			
6	+	+	+						0	+	+			
7	+	+	+	+					0	–	–			
8	+	+			+		+		0	–	–			
9	+	+			+	+	+		0	–	–			
10	+	+			+		+	+	0	–	–			
11	+	+			+	+	+	+	0	–	–			
12	+	+	+		+				0	–	–			
13	+	+	+		+	+			0.018	+	+	+		
14	+	+	+	+	+				0	+	+			
15	+	+	+	+	+	+			0.101	+	+	+	+	+
16	+	+	+				+		0	+	+			
17	+	+	+				+	+	0	+	+			
18	+	+	+	+			+		0	+	+			
19	+	+	+	+			+	+	0.010	+	+	+		
20	+	+	+		+		+		0	–	–			
21	+	+	+		+		+	+	0	–	–			
22	+	+	+		+	+	+		0.044	–	–			
23	+	+	+	+	+		+		0	–	+			
24	+	+	+		+	+	+	+	0.005	–	–			
25	+	+	+	+	+		+	+	0.251	–	–			
26	+	+	+	+	+	+	+		0.024	–	+			
27	+	+	+	+	+	+	+	+	0	–	–			
28	+	+	$=K_{dgxh}$		+	+			0.064	+	+	+	+	
29	+	+	$=K_{dgxh}$	$=K_{dgxhh}$	+	+			0.471	+	+	+	+	+
30	+	+	$=K_{dgxh}$	$=K_{dgxhh}$	+	+	$=K_{dgxh}$	$=K_{dgxhh}$	0.010	+	+	+		

[a] Dissociation constants for host–guest binding steps shown in Scheme 2. The plus sign indicates that the given step was included in the given binding mechanism. [b] Akaike weights (see text for details). [c] A plus sign indicates that formal standard errors of all adjustable model parameters were smaller than the parameter value itself. [d] A plus sign indicates that all adjustable intrinsic chemical shifts were within physically realistic bounds. [e] For an explanation of the plus signs see text.

Firstly, we computed the Akaike weight[15] of each model, as a statistical probability (between zero and one) that the given model is the "true" model. The Akaike weight takes into account not only the residual sum of squares for each model, but, importantly, also the number of adjustable model parameters; models containing larger numbers of adjustable parameters—in this case dissociation constants and intrinsic chemical shifts—are disadvantaged in the computation of the Akaike weight. The Akaike weights for each model are summarized in Table 2.

As a second criterion for model acceptance, we examined the statistical uncertainties of the adjustable model parameters, as measured by their formal standard errors. If any fitting model produced extremely large uncertainties in adjustable parameters, such that the formal standard error of any parameter appeared nominally larger than the best-fit value of the parameter itself, we rejected the model as over-parameterized. Failing this criterion is represented by a minus sign in the column labeled "errors" in Table 2.

Thirdly, we examined the best-fit values of intrinsic chemical shifts, treated as adjustable model parameters, to see if they fall within a physically plausible range. For some models, the nominal values of the intrinsic chemical shifts of the aromatic protons were essentially indeterminate, for example, larger than ten or smaller than one. If so, the given model was excluded even if the formal standard errors of all model parameters were relatively small.

The three columns labeled "$Pass_{x\%}$" in Table 2 indicate whether or not the candidate fitting model passes all three acceptance criteria simultaneously. If the Akaike weight of the given mechanism was larger than 0.01, representing at least 1% statistical probability of being the "true" model, *and* if the model passed the two remaining criteria, low standard errors and physically plausible chemical shifts, we placed a plus sign in the column labeled "$pass_{1\%}$". Similarly, we placed a plus sign in the column "$pass_{5\%}$" or "$pass_{10\%}$" if the Akaike weight was larger than 0.05 and 0.10, respectively, provided the remaining two model-acceptance criteria were also satisfied.

The results summarized in the last three columns of Table 2 show that only two models (models 15 and 29) out of 30 possible candidate mechanisms passed the model-acceptance test at greater than 10% probability level. However, the only difference between these two mechanisms is that in one case (model 15) there were four independent dissociation constants assigned to four different binding steps, whereas, in the other case (model 29), there were two pairs of degenerate equilibrium constants assigned to the same four steps.

Table 3. Second-pass model discrimination analysis for six possible DB24C8/paraquat binding mechanisms and the corresponding 95% confidence level intervals for equilibrium constants.

	Model 13	Model 15	Model 19	Model 28	Model 29	Model 30
K_{dgxxh}[a] [mM]	0.6–1.2	0.4–1.0	0.4–0.6	$=K_{dgxh}$	$=K_{dgxh}$	$=K_{dgxh}$
K_{dgxxhh}[a] [mM]	–	5.0-19.3	5.9-14.9	–	$=K_{dgxhh}$	$=K_{dgxhh}$
K_{dgxh}[a] [mM]	0.6–1.2	0.7–3.2	–	0.7–0.9	0.7–0.9	0.7–0.9
K_{dgxhh}[a] [mM]	2.4–6.7	2.5-13.8	–	3.5–4.8	5.5–9.5	5.6-12.8
K_{dgh}[a] [mM]	–	–	0.1–0.2	–	–	$=K_{dgxh}$
K_{dghh}[a] [mM]	–	–	3.1-18.5	–	–	$=K_{dgxhh}$
n_D[b]	153	153	153	153	153	153
n_P[c]	15	20	20	14	18	26
SS_{rel}[d]	1.21	1.08	1.12	1.21	1.10	1.00
ΔAIC_c[e]	6.3	3.1	7.7	3.9	0	7.9
weight[f]	0.03	0.14	0.02	0.10	0.70	0.01

[a] Dissociation constants for host–guest binding steps shown in Scheme 2. [b] Number of data points. [c] Number of optimized model parameters. [d] Relative sum of squares (lowest value among all models is set to unity). [e] Difference second-order AIC_c (lowest value among all candidate is set to zero). [f] Akaike weight.

To gain yet further insight into the nature of the binding mechanism, we determined the non-symmetrical confidence intervals,[14] at the 95% likelihood level, of all equilibrium constants appearing in the top six candidate models (models 13, 15, 19, 28, 29, and 30 in Table 2). These are all models for which the Akaike weights were greater than 0.01. The results are summarized in Table 3, which lists not only the confidence intervals but also the second-pass model discrimination analysis in terms of Akaike weights for each of the six second-pass models.

The most plausible model (Akaike weight 0.70) is model 29, in which the monocation and the electrically neutral paraquat molecule both bind to the crown ether with 1:1 and 2:1 stoichiometries. Additionally, model 29 stipulates that both the monocation and the electrically neutral paraquat molecule have exactly the same binding affinity as measured by the 1:1 and 2:1 dissociation constants. In order of the Akaike weights, that is, the statistical probabilities that the given model is the "true" model, this mechanism is again followed by model 15, in which the four dissociation constants are treated as independent parameters, but otherwise it is identical to model 29.

From the point of view of model discrimination, as it relates to confidence intervals for model parameters, it is important to note that the confidence intervals for two pairs of equilibrium constants appearing in model 15 (namely K_{dgxh}/K_{dgxxh} and K_{dgxhh}/K_{dgxxhh}) overlap, and therefore are essentially identical within the 95% likelihood level. Thus, considering this numerical equivalence of both K_{dgxh}/K_{dgxxh} and K_{dgxhh}/K_{dgxxhh} pairs, model 15 in fact reduces to model 29.

It is also important to note that the 95% confidence intervals for certain equilibrium constants appearing in Table 3 are essentially identical irrespective of the postulated mechanism. For example, the equilibrium dissociation constant for the 1:1 host–guest complex formed by the paraquat monocation, K_{dgxh}, falls between 0.7 and 0.9 mM (at the 95% confidence level) for three of the six mechanisms. In model 13, the range of plausible values is somewhat larger, but still relatively small, $K_{dgxh}=(0.6–1.2)$ mM. Only in the borderline over-parameterized model 15 does the confidence interval widen to $K_{dgxh}=(0.7–3.2)$ mM. However, this somewhat wider range is still compatible with estimates of K_{dgxh} generated from all five remaining models.

Discussion

Ionization of paraquat in [D6]acetone: The ionization of paraquat in [D_6]acetone was previously studied by Huang et al.[6,19] who elected to use a simplified mathematical model based on the assumption that only two states of paraquat were present in [D_6]acetone, namely, the neutral molecule and the fully ion-dissociated dication. In our work, we have chosen a fully general numerical model for the statistical analysis of our experimental data, avoiding the involvement of any simplifying assumptions or restrictions on the total number of either component species or the molecular complexes they form.

We have analyzed the changes in the chemical shifts of the aromatic protons as the populations of the three states of paraquat—the neutral, mono-, and dicationic species—were methodically altered. These changes in chemical shift can be observed (Figure 3A,B) by simply diluting paraquat in [D_6]acetone. Preliminary statistical analyses of the dilution data showed that the dilution experiment alone does not provide sufficient information about the two stepwise dissociation constants, K_{dgxx} and K_{dgx} in Scheme 1. Only a perturbation (Figure 3C,D) of the paraquat–counterion system, obtained by adding additional hexafluorophosphate salt, allowed us to determine the numerical values (Table 1) of both dissociation constants.

Our physical model of the stepwise ionization of paraquat is also supported by the best-fit value of the dissociation constant for Bu_4NPF_6. According to our regression analysis, this dissociation constant is $K_{dnx}=(11.9\pm2.5)$ mM. Goldfarb et al.[20] determined the association constant of Bu_4NPF_6 in acetone at 25°C from conductivity measurements as $K_A=1/K_d=(78\pm4)\,M^{-1}$, which corresponds to $K_{dnx}\approx(12.8\pm0.7)$ mM. Within the associated formal standard error, this value is essentially identical to the value of K_d determined in our work from ^{1}H NMR spectroscopic data. The close agreement between K_d for Bu_4NPF_6, determined experimentally in our work (11 mM), and the corresponding value (12.8 mM) previously reported in the literature,[20] suggests that either the mean activity coefficients are close to unity, or that any discrepancies between concentrations and activities can be neglected, within the experimental error, in the concentration range used in this study (see the Supporting Information). In any case, the close agreement between our

experimentally determined value for the dissociation constant of Bu_4NPF_6 with the published value lends strong support to other aspects of our paraquat dissociation model, namely, the numerical values of the ionization constants K_{dgxx} and K_{dgx} in Scheme 1.

Huang et al. have argued in their original report,[6] as well as in a more recent publication,[19] against the presence of the paraquat monocation in [D_6]acetone. In both reports, it is argued that, under the typical experimental conditions used in host–guest complexation studies ($[GX_2]_0 < 30$ mM), paraquat in [D_6]acetone exists predominantly as the fully ion-associated neutral molecule. Presumably, paraquat sheds its counterions only in the presence of the crown ether complexation agent, resulting in doubly charged pseudorotaxane complexes.[6,19] Our experimental data, the best-fit ionization model shown in Figure 3, and the attempted fit (Figure 5) to the single-step ionization mechanism proposed by Huang et al. clearly contradict this hypothesis. In fact, from the data presented in Figure 3, we have determined experimentally that the paraquat monocation is the most highly populated species, existing at total concentrations ranging from $[GX_2]_0 = 0.5$ mM to $[GX_2]_0 = 20$ mM (see Figure 4). Given this result, it seems reasonable to expect that the monocation, as the most abundant species of paraquat, would participate, to at least some degree, in the formation of host–guest complexes. Indeed, in our DB24C8/paraquat complexation studies, we have shown that the paraquat monocation is significantly involved in host–guest complexation.

Mathematical modeling of complex simultaneous equilibria: Considering that paraquat in acetone undergoes stepwise dissociation ($GX_2 \rightleftharpoons GX^+ + X^- \rightleftharpoons G^{2+} + 2X^-$) and allowing for up to 2:1 host–guest complexation stoichiometry—involving each of the three separate forms of paraquat (GX_2, GX^+, and G^{2+})—leads to 26 unique complexation mechanisms. It has been pointed out[19] that "the mathematical treatments of these scenarios are complex and not readily solved in closed form." In fact, a mathematically more precise statement would be that no closed-form (algebraic) mathematical treatment can exist at all, in principle, for any of the 26 possible complexation mechanisms generated from Scheme 2. In other words, no single "fitting equation" or "binding isotherm" can ever be derived for any of these 26 binding mechanisms.

For this reason, we have entirely abandoned the traditional algebraic treatment of host–guest complexation equilibria, and have chosen instead a fully general numerical, or iterative, method. The classic computational algorithm EQUIL[8] solves a complete *system* of simple nonlinear algebraic equations, each one representing the mass balance for one particular constituent (component) molecular species. This approach allows any arbitrary binding mechanism to be treated mathematically. Many similar computational algorithms have been described in the literature[21] on complex chemical equilibria. We chose the particular algorithm EQUIL[8] because it is conveniently implemented in the software package DynaFit.[9] This tool allowed us to specify each theoretical fitting model, not as a set of simultaneous nonlinear equations, but rather as a set of chemical equations entered as text; for example, `G.X.X<==>G.X+X<==>G+X+X` for stepwise paraquat dissociation, or `G.X+H<==>G.X.H+H<==>G.X.H.H` for the simultaneous 1:1 and 1:2 binding of DB24C8 to the paraquat monocation. The DynaFit package[9] automatically derives each underlying mathematical model.

Molecular mechanism of DB24C8/paraquat complexation: A necessary prerequisite for the study of DB24C8/paraquat complexation was to establish independently the paraquat counterion dissociation mechanism, as well as the numerical values of the relevant dissociation constants—K_{dgxx} and K_{dgx} in Scheme 1. We accomplished this task by conducting a series of NMR experiments, in which either the total paraquat concentration or, in addition, the counterion concentration was varied. In this way, we were able to control the mole fractions of the three paraquat species present in [D_6]acetone (see Figure 3).

We have used the same "counterion-perturbation method" in our host–guest complexation investigations. We created ternary mixtures of host, guest, and counterion—as the tetrabutylammonium salt—and recorded the ^{1}H NMR chemical shifts of all four aromatic protons in the DB24C8/paraquat system. In fact, the global fit[10] of chemical shifts for all four aromatic protons, combined together and analyzed as a single data set, proved to be the key to a successful model discrimination analysis. In our preliminary studies, when the chemical shifts for each proton were analyzed separately, no model discrimination was possible, because there was not enough information—in the information–theoretic sense[15]—about the underlying model. We note that other workers studying DB24C8/paraquat complexation[6,19] use NMR chemical shift data for only a single proton resonance. The experimental data and the best-fit complexation model (model 29 in Table 2) are shown in Figure 6.

Of the 30 candidate binding models listed in Table 2, several complexation mechanisms describe our experimental data approximately equally well, at least as measured by the second-order AIC_c.[15] See also Table 3 for a list of these six most plausible models. However, no theoretical model for any observable physical phenomenon can ever be ultimately proved as the "true" or "final" model. Indeed, the ultimate goal of the model-building exercise is to *exclude* from further consideration all those theoretical models that clearly contradict the available experimental data. By this measure, we consider our having reduced the comprehensive list of all 30 complexation models to a handful of closely related candidates as a considerable success.

More specifically, we were able to exclude as clearly implausible the DB24C8/paraquat complexation model previously proposed by Huang et al.[6,19] Their proposed model has the following important characteristics: 1) in solutions of paraquat in [D_6]acetone—in the absence of the crown ether host—paraquat exists exclusively in one of two forms, either as a fully associated neutral molecule or as a fully dissociated dication; 2) only the paraquat dication binds to the crown ether host; and 3) no other molecular species are

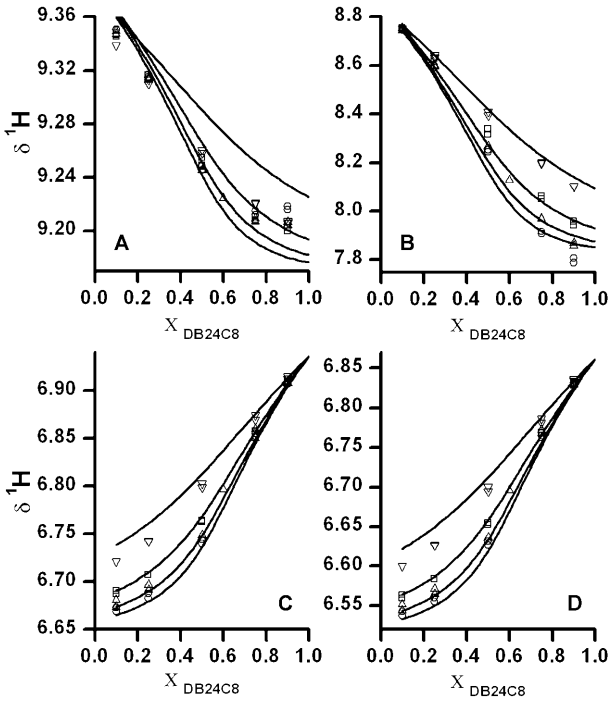

Figure 7. Least-squares fit of paraquat and DB24C8 chemical shifts to the 1:1 complexation model proposed by Huang et al.[6] See legend to Figure 6 for other details.

present in solution. The least-squares fit of our counterion-perturbation data to a mathematical model derived from these assumptions is shown in Figure 7. Even without conducting any rigorous statistical analyses—for example, by comparing the AIC_c value for the competing models—we see in Figure 7 that the "best-fit" model and the experimental data clearly disagree. It follows that the previously proposed mechanism of DB24C8/paraquat complexation[6,19] has now been invalidated by our experimental counterion-perturbation study.

We have also attempted to perform a model-discrimination analysis of the previously published chemical shift data.[6] We found that these data are indeed fully compatible with the single-step mechanism for paraquat dissociation and with the hypothesis of "counterion-driven" host–guest complexation.[6] As the authors correctly state in a subsequent publication,[19] their simplified mathematical model provides a "reasonably satisfactory" fit.

We explain the discrepancies in the mechanistic conclusions drawn either from the published chemical shifts or from our own data as arising from several contributing factors.

Firstly, the authors[6] analyzed only the chemical shifts recorded for a single proton, whereas we have analyzed globally[10] the chemical shifts for all four aromatic protons combined. Indeed, certain subsets of our own experimental data—but only when analyzed separately for each proton—do conform perfectly well to the previously published simplified mechanism.[6] In our hands, global analysis was the key to successful model discrimination.

Secondly, the authors[6] performed their binding study in the absence of any added counterion (as Bu_4NPF_6), whereas we have purposely modulated the relative abundance of paraquat species by employing the counterion-perturbation method. The multiple paraquat species (Scheme 2), both unbound in solution and bound in variously charged pseudorotaxanes, became experimentally detectable only when perturbed in this systematic way.

Finally, we used rigorous statistical model discrimination techniques[15] to assess the validity of each of our 30 candidate models quantitatively. Without using such quantitative assessments of model validity, any notion of a "reasonably satisfactory" agreement[19] between the data and the model remains purely subjective.

It is worth noting that according to our statistical model discrimination analysis, the paraquat dication (G^{2+}) is not involved in the two most-plausible binding models (models 15 and 29 in Table 2). This situation contradicts chemical intuition, since one would assume the two positive charges on this guest molecule would increase its affinity for electron-rich hosts. However, G^{2+} is a very minor species under the conditions of our investigation (see Figure 4 for the distribution of all three species), and therefore the data do not contain much information with regard to G^{2+}'s binding with DB24C8. However, while our data does not explicitly support the involvement of G^{2+}, its participation in host–guest complexation cannot be excluded by our data either. This caution on our part is signified by the question marks in Figure 8. In order to assess the involvement of the

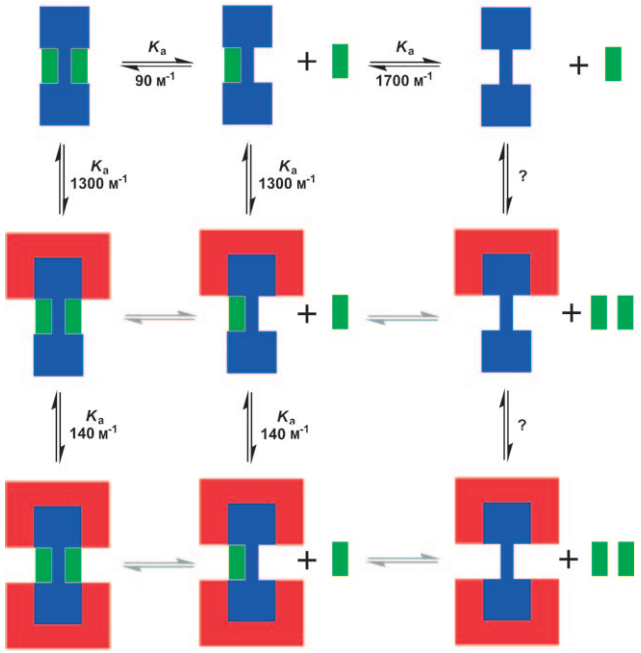

Figure 8. Graphical representation of the complexation and ionization equilibria involved in the DB24C8/paraquat system. The numerical values are association constants ($м^{-1}$) that were established in this study. The question marks identify binding steps that can neither be confirmed nor excluded, given the limitations of the available experimental data.

paraquat dication definitively in complexation with DB24C8, further experiments would be required. We performed preliminary simulations using the software package DynaFit,[9] with the aim of determining the optimal experimental design for such additional studies. Based on these preliminary results, a significant number of additional NMR spectra would have to be recorded, specifically at low total concentrations of paraquat ($[GX_2]_o < 1$ mM, preferably between 0.05 and 0.5 mM). In this particular concentration range, the mole fraction of the paraquat dication G^{2+} is relatively high (see Figure 4), and therefore its complexation characteristics could be studied. Unfortunately, at total concentrations below 1 mM, the sensitivity of the NMR detection method significantly deteriorates. In order to continue our investigations, it may be necessary to use another detection method.

Conclusions

We have deployed both theoretical methods and experimental techniques that go beyond those previously employed[6] to study the host–guest complexation system between paraquat bis(hexafluorophosphate) and dibenzo[24]crown-8. On the theoretical and computational front, we have implemented a general mathematical formalism for the modeling of simultaneous equilibria[8] that does not require us to make any simplifying assumptions. Using this numerical, as opposed to an algebraic, approach and suitable software tools that implement it,[9] we were able to build 30 different mathematical models for DB24C8/paraquat complexation and compared their relative merits in fitting them to the experimental data. Our model selection strategy was based on rigorous information–theoretic measures of model adequacy, namely, the second-order AIC_c.[15] The nonsymmetrical confidence intervals of model parameters[14] also played an important role in model selection, as did the global fit[10] strategy of pooling the chemical shifts of all four aromatic protons.

On the experimental front, we employed the "counterion perturbation" method, using an additional counterion (as the ammonium salt) to shift purposely the equilibria involving paraquat, *and* the corresponding host–guest complexes, in either direction. In this way, we were able to detect unambiguously the presence of both 1:1 complexes and of 2:1 (host/guest) complexes in solution. The formation of 2:1 complexes in solution is reminiscent of the 2:1 "taco" complexes that have been reported previously to exist in the solid state.[6,22] The 2:1 complexes are formed more weakly (binary association constants $\sim 100\,M^{-1}$) than the 1:1 complexes (binary association constants $\approx 1000\,M^{-1}$).

Both the paraquat monocation and the neutral molecule form their complexes with approximately identical binding affinities toward the crown ether. See the numerical values of the dissociation constants in Table 3. It follows that the same extent of ion-pairing must exist for paraquat, either unbound in solution or bound to the crown ether. The relative magnitude of the equilibrium constants summarized in Table 3 suggests that the most abundant host–guest complex is the DB24C8/paraquat monocation, just as the most abundant species of unbound paraquat in [D$_6$]acetone is singly charged. Thus, in the particular case of DB24C8/paraquat binding interactions, ion-pairing does not influence or "drive" the formation host–guest complexes, as was previously assumed.[6]

Experimental Section

Chemicals were purchased commercially and used without further purification. Paraquat bis(hexafluorophosphate) was prepared according to literature procedures.[7] NMR spectroscopy was performed on a Bruker DRX500 (500 MHz) or an Avance 600 (600 MHz) spectrometer at ambient temperature (22 °C). The reported chemical shifts are measured relative to the residual solvent peak in [D$_6$]acetone ($\delta = 2.05$ ppm). Solutions for NMR spectroscopic analysis were obtained as follows. A stock solution of tetrabutylammonium hexafluorophosphate was prepared by weighing out a precise mass into a Corning 5630 volumetric flask, and subsequently adding deuterated solvent to the graduation line. Two separate stock solutions of paraquat bis(hexafluorophosphate) and DB24C8 were then prepared by weighing out a precise mass of each compound in separate volumetric flasks, and then adding the previously prepared solution of tetrabutylammonium hexafluorophosphate in deuterated acetone to the graduation line. Precise combinations of each stock solution were then added directly to 7" NMR tubes with Fisherbrand Finnpipette II single-channel pipetters. This protocol produced solutions containing well-defined concentrations of paraquat bis(hexafluorophosphate) and DB24C8 at different constant concentrations of tetrabutylammonium hexafluorophosphate for NMR spectroscopic analysis and subsequent analytical data processing.

Acknowledgements

The collaboration was supported by the Microelectronics Advanced Research Corporation (MARCO, J.F.S.) and its focus centers on Functional Engineered NanoArchitectonics (FENA) and Materials Structures and Devices, and the Center for Nanoscale Innovation for Defense (CNID, J.F.S.). J.M.S. thanks the NSF for a Graduate Research Fellowship. T.B.G. acknowledges the NSF-IGERT scheme gratefully for a Materials Creation Training Program (MCTP) Traineeship.

[1] a) J. D. Badjić, V. Balzani, A. Credi, S. Silvi, J. F. Stoddart, *Science* **2004**, *303*, 1845–1849; b) V. Balzani, A. Credi, F. M. Raymo, J. F. Stoddart, *Angew. Chem.* **2000**, *112*, 3484–3530; c) V. Balzani, A. Credi, M. Venturi, *Molecular Devices and Machines—A Journey into the Nano World*, 2nd ed., Wiley-VCH, Weinheim, **2008**; d) C. P. Collier, J. O. Jeppesen, Y. Luo, J. Perkins, E. W. Wong, J. R. Heath, J. F. Stoddart, *J. Am. Chem. Soc.* **2001**, *123*, 12632–12641; e) J.-P. Collin, V. Heitz, J.-P. Sauvage, *Top. Curr. Chem.* **2005**, *262*, 29–62; f) M. R. Diehl, D. W. Steuerman, H.-R. Tseng, S. A. Vignon, A. Star, P. C. Celestre, J. F. Stoddart, J. R. Heath, *ChemPhysChem* **2003**, *4*, 1335–1339; g) D. W. Steuerman, H.-R. Tseng, A. J. Peters, A. H. Flood, J. O. Jeppesen, K. A. Nielsen, J. F. Stoddart, J. R. Heath, *Angew. Chem.* **2004**, *116*, 6648–6653; *Angew. Chem. Int. Ed.* **2004**, *43*, 6486–6491; h) H. B. Yu, Y. Luo, K. Beverly, J. F. Stoddart, H.-R. Tseng, J. R. Heath, *Angew. Chem.* **2003**, *115*, 5884–5889; *Angew. Chem. Int. Ed.* **2003**, *42*, 5706–5711.

[2] M. C. T. Fyfe, P. T. Glink, S. Menzer, J. F. Stoddart, A. J. P. White, D. J. Williams, *Angew. Chem.* **1997**, *109*, 2158–2160; *Angew. Chem. Int. Ed. Engl.* **1997**, *36*, 2068–2070.

[3] J. W. Choi, A. H. Flood, D. Steuerman, S. Nygaard, A. B. Braunschweig, N. N. P. Moonen, B. W. Laursen, Y. Luo, E. DeIonno, A. J. Peters, J. O. Jeppesen, K. Xu, J. F. Stoddart, J. R. Heath, *Chem. Eur. J.* **2006**, *12*, 261–279.
[4] a) A. H. Flood, J. F. Stoddart, D. W. Steuerman, J. R. Heath, *Science* **2004**, *306*, 2055–2056; b) Y. Luo, C. P. Collier, J. O. Jeppesen, K. A. Nielsen, E. DeIonno, G. Ho, J. Perkins, H. R. Tseng, T. Yamamoto, J. F. Stoddart, J. R. Heath, *ChemPhysChem* **2002**, *3*, 519–525; c) J. E. Green, J. W. Choi, A. Boukai, Y. Bunimovich, E. Johnston-Halperin, E. DeIonno, Y. Luo, B. A. Sheriff, K. Xu, Y. S. Shin, H. R. Tseng, J. F. Stoddart, J. R. Heath, *Nature* **2007**, *445*, 414–417.
[5] a) R. Arnecke, V. Böhmer, R. Cacciapaglia, A. D. Cort, L. Mandolini, *Tetrahedron* **1997**, *53*, 4901–4908; b) S. Bartoli, S. Roelens, *J. Am. Chem. Soc.* **1999**, *121*, 11908–11909; c) P. D. Beer, M. R. Sambrook, D. Curiel, *Chem. Commun.* **2006**, 2105–2117; d) V. Böhmer, A. D. Cort, L. Mandolini, *J. Org. Chem.* **2001**, *66*, 1900–1902; e) M. Clemente-León, C. Pasquini, V. Hebbe-Viton, J. Lacour, A. D. Cort, A. Credi, *Eur. J. Org. Chem.* **2006**, 105–112; f) C. A. Hunter, C. M. R. Low, C. Rotger, J. G. Vinter, C. Zonta, *Chem. Commun.* **2003**, 834–835; g) M. Montalti, L. Prodi, *Chem. Commun.* **1998**, 1461–1462; h) G. V. Oshovsky, D. N. Reinhoudt, W. Verboom, *Eur. J. Org. Chem.* **2006**, 2810–2816.
[6] F. Huang, J. W. Jones, C. Slebodnick, H. W. Gibson, *J. Am. Chem. Soc.* **2003**, *125*, 14458–14464.
[7] A. Manjula, M. Nagarajan, *ARKIVOC* **2001**, *viii*, 165–183.
[8] T.-P. I, G. H. Nancollas, *Anal. Chem.* **1972**, *44*, 1940–1950.
[9] P. Kuzmic, *Anal. Biochem.* **1996**, *237*, 260–273.
[10] J. M. Beechem, *Methods Enzymol.* **1992**, *210*, 37–54.
[11] J.-G. Reich, *Curve Fitting and Modeling for Scientists and Engineers*, McGraw-Hill, New York, **1992**.
[12] D. W. Marquardt, *J. Soc. Ind. Appl. Math.* **1963**, *11*, 431–441.
[13] K. V. Price, R. M. Storm, J. A. Lampinen, *Differential Evolution—A Practical Approach to Global Optimization*, Springer, Heidelberg, **2005**.
[14] D. M. Bates, D. G. Watts, *Nonlinear Regression Analysis and its Applications*, Wiley, New York, **1988**.
[15] K. P. Burnham, D. R. Anderson, *Model Selection and Multimodel Inference: A Practical Information-Theoretic Approach*, 2nd ed., Springer, Heidelberg, **2002**.
[16] a) P. Job, *Ann. Chim.* **1928**, *9*, 113–203; b) V. M. S. Gil, N. C. Oliveira, *J. Chem. Educ.* **1990**, *67*, 473–478; c) R. Sahai, G. L. Loper, S. H. Lin, H. Eyring, *Proc. Natl. Acad. Sci. USA* **1974**, *71*, 1499–1503.
[17] a) R. L. Buckson, S. G. Smith, *J. Phys. Chem.* **1964**, *68*, 1875–1878; b) A. K. Covington, M. L. Hassall, I. R. Lantzke, *J. Chem. Soc. Faraday Trans. 2* **1972**, *68*, 1352–1358; c) P. Haake, R. V. Prigodich, *Inorg. Chem.* **1984**, *23*, 457–462; d) M. Krell, M. C. R. Symons, J. Barthel, *J. Chem. Soc. Faraday Trans. 1* **1987**, *83*, 3419–3427; e) Y.-Y. Lim, R. S. Drago, *J. Am. Chem. Soc.* **1972**, *94*, 84–90; f) R. P. Taylor, I. D. Kuntz, *J. Am. Chem. Soc.* **1969**, *91*, 4006–4007.
[18] K. B. Burnham, D. R. Anderson, *Model Selection and Multimodel Inference: A Practical Information-Theoretic Approach*, 2nd ed., Springer, Heidelberg, **2002**.
[19] F. Huang, J. W. Jones, H. W. Gibson, *J. Org. Chem.* **2007**, *72*, 6573–6576.
[20] D. L. Goldfarb, M. P. Longinotti, H. R. Corti, *J. Solution Chem.* **2001**, *30*, 307–322.
[21] W. R. Smith, R. W. Missen, *Chemical Reaction Equilibrium Analysis: Theory and Algorithms*, Wiley-Interscience, New York, **1982**.
[22] P. R. Ashton, S. J. Langford, N. Spencer, J. F. Stoddart, A. J. P. White, D. J. Williams, *Chem. Commun.* **1996**, 1387–1388.

Received: September 4, 2008

